# THE MEES CCD IMAGING SPECTROGRAPH

MATTHEW J. PENN, DONALD L. MICKEY, RICHARD C. CANFIELD, and BARRY J. LABONTE

*Institute for Astronomy, University of Hawaii, Honolulu, HI 96822, U.S.A.*

(Received 22 December, 1990; in revised form 11 March, 1991)

**Abstract.** The Mees CCD (MCCD) instrument is an imaging spectroscopy device which uses the 25 cm coronagraph telescope and the 3.0 m Coudé spectrograph at Mees Solar Observatory (MSO) on Haleakala, Maui. The instrument works with resolving power up to $R \approx 200\,000$ with significant throughput from $\lambda$3934 Å (Ca II K) to $\lambda \approx 10\,000$ Å. A fast guiding active mirror stabilizes the image during observations. A rapidly writing magnetic tape storage system allows observations to be recorded at 256 kbytes $s^{-1}$. Currently, the MCCD is used for imaging spectroscopy of solar flares at $\lambda$6563 Å (H$\alpha$), and velocity measurements of umbral oscillations; future plans include emission line studies of active region coronae, and photospheric studies of solar oscillations.

## 1. Introduction

The scientific goals of the MCCD are varied, and range from observing the slow evolution of active region coronae to providing spectroscopic diagnostics during rapid chromospheric flares. At peak performance, over a 10 hour observing day, the MCCD was intended to make 30 ms exposures, each with 0.6 arc sec spatial resolution, and 14 mÅ spectral resolution. These goals placed new demands on the image quality, system throughput, spatial and spectral stability of the coronagraph and spectrograph instrument package.

The coronagraph and spectrograph instruments have been used in many ways since their installation in 1970. Photographic coronal work was done with these instruments (Fisher, 1971a, b; Fisher and Pope, 1971; McCabe, 1973) which was aimed at understanding the spatial and velocity distribution of coronal plasma as observed in several different spectral lines. Various spectrophotometric observations were made with the intention of studying the physical properties of prominences, (Landman, 1976, Landman, Edberg, and Laney, 1977; Landman, Illing, and Mongillo, 1978; Landman, 1981b, 1985; Brickhouse and Landman, 1987) and solar plage (Landman, 1981a; LaBonte, 1986a, b). Photospheric and chromospheric solar oscillations were investigated in two projects, with time series observations of the solar spectrum around C I $\lambda$5380 Å (Lindsey and Landman, 1980) and He D3 $\lambda$5876 Å (Landman, 1981a). These projects encompass most of the observations made with the coronagraph and spectrograph instrument package.

Although these instruments have been used for many years, there is no comprehensive reference which describes them. For this reason, we review the 25 cm coronagraph telescope and 3.0 m Coudé spectrograph system in Section 2. We describe, in Section 3, the characterization of the instrument package, and the adjustments made to meet MCCD requirements. In Sections 4 and 5, we explain the optical and electronic systems

*Solar Physics* **135:** 163–177, 1991.

that comprise the MCCD instrument. We discuss two current observing programs run with the MCCD in Section 6, and lastly, in Section 7, we list several future observing programs, and discuss potential uses for the MCCD instrument in solar astronomy.

## 2. The Coronograph-Spectrograph Instruments from 1969 to 1987

The 25 cm coronagraph telescope and 3.0 m Coudé spectrograph instrument package was built by Boller and Chivens in 1967. The installation of the telescope on the 3.7 m solar spar, and the spectrograph in the Coudé room of MSO was completed in 1970. In this section, we describe the design and features of each of these instruments prior to the MCCD project.

The coronagraph telescope (see Figure 1) employs a singlet 25 cm diameter, 355 cm focal length objective lens ($L1$). At the prime focus of this lens is a two-turret collection

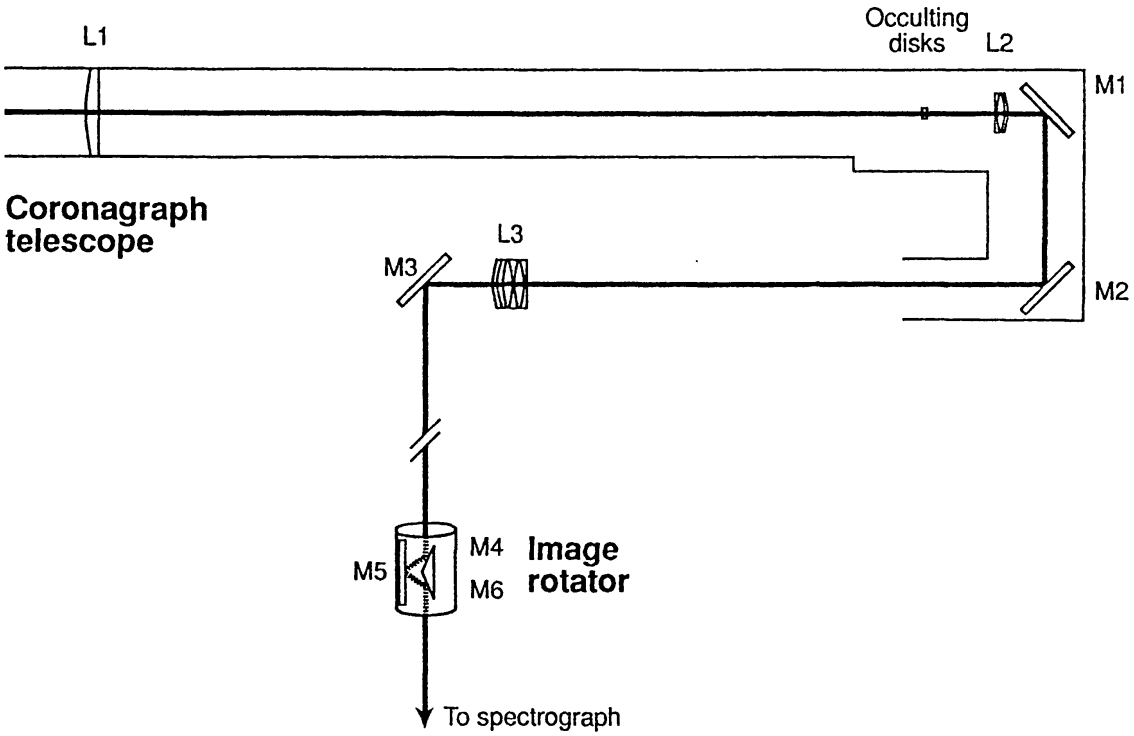


Fig. 1. Optical diagram of the 25 cm coronagraph telescope. At the focus of the objective ($L1$) is a selection of occulting disks which allow the corona to be observed. The second objective ($L3$) corrects for the chromatic aberration of the telescope. The Coudé mirror ($M3$) directs the sunlight into the image rotator, which removes rotation from the image plane. In the current setup, the MCCD optical bench immediately follows the image rotator (see Figure 4).

of occulting disks, which can occult any section of the solar limb. Light from the photosphere is reflected off these occulting disks and out of the telescope when the solar corona is being observed. A field lens ($L2$) following the prime focus forms a pupil image on a second objective lens ($L3$). Two fold mirrors ($M1$ and $M2$) fold the beam towards the center of the spar mount. The second objective ($L3$) is a hyperchromatic lens, and corrects for the chromatic aberration of the coronagraph lenses. After the $L3$, the beam

reflects off a steerable Coudé mirror ($M3$) to an image plane on the slit of the spectrograph in the Coudé room. The image scale is 27 arc sec $mm^{-1}$. Just before the image plane, a three mirror image rotator ($M4$ through $M6$), directly driven by the spar removes image rotation at the Coudé focus.

The 3.0 m focal length Coudé spectrograph (see Figure 2) receives a solar image from

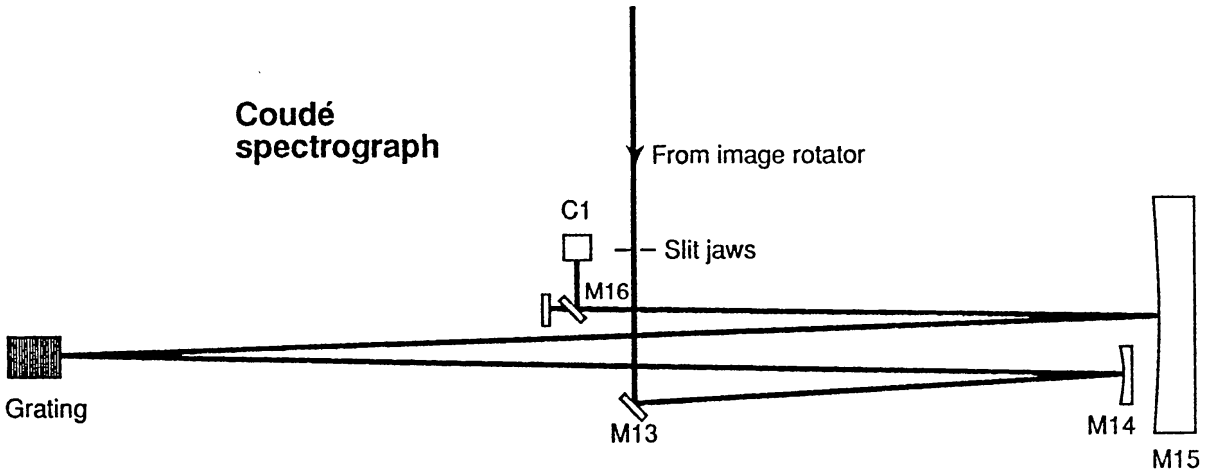


Fig. 2. Optical diagram of the 3.0 m Coudé spectrograph. The slit jaws allow sunlight to enter the spectrograph, which is collimated by $M14$, dispersed by the diffraction grating, and focused by the camera mirror, $M15$. A small flat mirror ($M16$) feeds part of the spectrum to the Photometrics CCD camera, $C1$.

the coronagraph at the slit jaw assembly. The slit jaws adjust from a width 10 μm up to several hundreds of μm. A flat folding mirror ($M13$) redirects the light to the collimating mirror ($M14$), which illuminates the diffraction grating with a collimated beam. One of two diffracting gratings disperse the light. The normal incidence grating (No. 1), ruled at 600 lines $mm^{-1}$, is blazed for use in first order with a focal plane reciprocal dispersion of 5.7 Å $mm^{-1}$. The echelle grating (No. 2) is ruled at 300 lines $mm^{-1}$, blazed for a 63°26′ angle of incidence, and provides reciprocal dispersions greater than 0.6 Å $mm^{-1}$. The camera mirror ($M15$) focuses the dispersed light on a curved focal plane, measuring 2.5 cm across the dispersion and 40 cm along the dispersion. Here, a 35 mm film transport can photographically record part or all of the solar spectrum. A small flat mirror ($M16$) directs the light to a viewport. An optional double-pass beam provides greater spectral purity and dispersion.

## 3. Characterizations of Telescope Performance and Subsequent Adjustments

We made measurements of sunspots with the MCCD instrument, and characterized the slow spatial image drift. This drift was determined to have two possible sources, either (1) spurious image rotation which would introduce translational motion after the image rotator, or (2) motion of optical elements in the light beam. In order to eliminate spurious image rotation, we adjusted the pointing of the spar polar axis, internally aligned the image rotator, and re-positioned the image rotator in the Coudé beam. Currently, the spar polar axis is measured to be within 60 arc sec of the pole, which introduces less

than one arc sec hour$^{-1}$ of spurious motion in the image plane. The image rotator was realigned using a standard technique (Kingslake, 1983), and measurements of the optical axis of the telescope made with the image rotator in the beam show that the maximum spurious translational motion introduced by the rotator is now less than 2 arc sec hour$^{-1}$. Two optical elements were found to be contributing to image motion. First, the coronagraph objective ($L1$) was discovered to be loose in its mounting cell, accounting for an anomalous image shift each day near local noon. Also, the mounting bracket for the Coudé mirror ($M3$) was found to be improperly balanced, and thus not properly correcting for the spar's declination motion. Currently, spurious image motion seen in the image plane is a few arc sec hour$^{-1}$, which probably results from residual imbalances in the Coudé mirror mount. This image motion is within the limits imposed by the MCCD design, and is completely removed by the fast guiding system.

From observations made in the steep wings of strong spectral lines we found that the spectrograph had high-frequency shaking problems, between frequencies of 1 to 3 s$^{-1}$. We investigated the shaking more precisely by finding shifts in a time series of zeroth-order slit jaw images produced by the flat field lamp. Almost all of the high-frequency shaking was eliminated when a refrigerating unit in the Coudé room and the air conditioning ducts of the building were mechanically isolated from the spectrograph. Low-frequency drift still exists in the spectrograph with a linear slope of 15 mÅ hour$^{-1}$, and Fourier analysis shows that its amplitude decreases smoothly with frequency, containing no resonances.

Two characterizations of the final operating MCCD system are shown in Figure 3; the spectrograph beam profile, and the system spectral response. The spectrograph beam profile shows that the spectral point spread function has a full width at half-max (FWHM) of 28 mÅ, which is near the diffraction limit of the spectrograph. The useful spectral range of the instrument extends from Ca II K $\lambda$3934 Å to $\lambda$10 000 Å, although it is possible to access regions both blueward and redward of this range.

## 4. MCCD Modifications I – The Optical Bench

The five major revisions to the optical system of the coronagraph spectrograph required for the MCCD project consisted of: (1) providing rapid, controlled exposures, (2) scanning the solar image on the spectrograph slit, (3) producing a live video image of the solar region being studied with the spectrograph, (4) stabilizing the image with a fast guiding system, and (5) providing calibration flat field images. The MCCD optical bench (shown in Figure 4) has 4 beams which fulfill these requirements. The main optical beam uses a shutter mirror and an image scanning mirror to make exposures and scan the solar image. The image monitor beam produces a live video image comparable to a slit jaw image. The fast guider beam provides a motion feedback signal used to stabilize the image, and finally, the flat field beam provides calibration source for the MCCD detectors.

The main optical beam of the optical table consists of five flat mirrors ($M7$–$M11$) and four Nikkor telephoto lenses ($L4$–$L7$). This beam forms two pupil images, one on

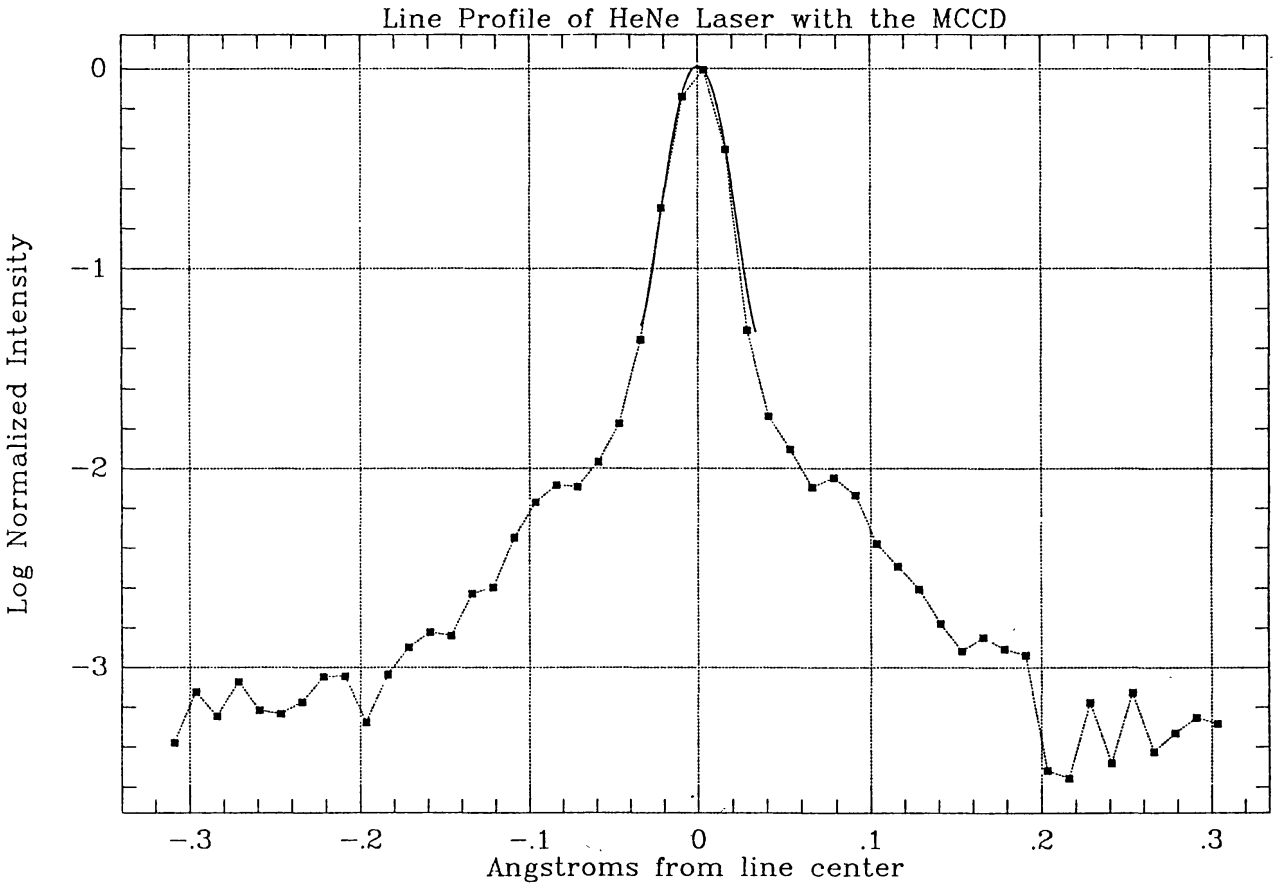


Fig. 3a. The response of the MCCD system to a HeNe laser beam at λ6328 Å. We used the echelle grating (No. 2) with a 42 μm slit and a long exposure of 100 s. A Gaussian fit to the observed line core (solid line in the figure) gives a full width at half-max (FWHM) of 28 mÅ. This implies that the spectral resolving power $R = \lambda/\delta\lambda = 226\,000$.

the active mirror ($M9$), and the other near the fast shutter ($M10$) and image scanning ($M11$) mirrors. The two associated image planes are located just before $M8$, and between $L5$ and $L6$. The shutter mirror ($M10$) is a flat mirror mounted on a galvanometer motor. When closed, the shutter mirror sends light into the image monitor bench, while open (removed from the beam) it allows light to pass to the scanner mirror and eventually to the spectrograph. The shutter motion is linear and stable down to exposures of 25 ms. The scanning mirror ($M11$) is used to scan the solar image across the spectrograph slit. This mirror is also mounted on a galvanometer motor, and can scan the entire field of view (several hundred arc sec) across the spectrograph slit in a few ms.

The image monitor beam of the optical table produces a live video display of the solar region observed by the spectrograph. The beam from the closed shutter mirror is re-imaged by a 50 mm Nikkor lens ($L8$) and enlarged to an appropriate image scale via a 75 mm Nikkor lens ($L9$). By repositioning this lens ($L9$) and the detector ($C2$), a range of image scales can be produced. A pentaprism ($P$) flips the image left to right to achieve the desired N–S–E–W image orientation, and various interference filters ($F$) can be

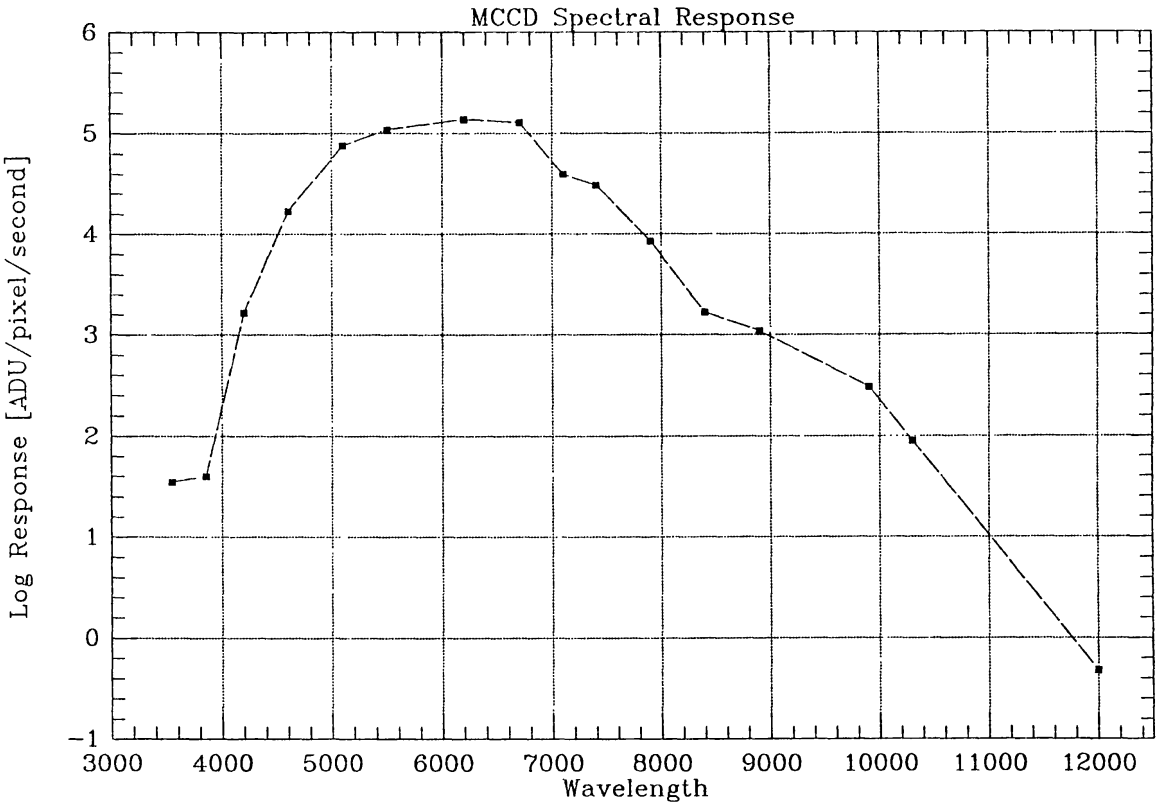


Fig. 3b. The spectral response of the MCCD from $\lambda$3550 Å to $\lambda$12000 Å. This graph shows the solar flux, in ADU (analog-digital units) per second per pixel, detected by the Photometrics CCD camera at the spectrograph focus. We observed several solar continuum regions at the center of the solar disk at local noon, with the normal incidence grating (No. 1) (with a dispersion of 8 pixels $Å^{-1}$) no pre-filters, and a 60 μm wide slit. From this graph we can calculate the exposure time needed for any observation, using simple linear extrapolations to the particular observational parameters. Note that the Photometrics camera saturates all 12 bits at a value of $\log_{10}(4095) \approx 3.6$.

positioned in the beam to isolate different wavelengths. The image plane detector ($C2$) for this beam is a Cohu video rate CCD camera.

A thin glass plate acts as a beam splitter (BS) and directs light out of the main beam into the fast guider beam. A section of the solar surface is selected by tilting the beam splitter. The zoom lens ($L11$) allows a variable image scale to be formed on the pointing camera ($C3$) and the position sensor (PS). Motion of a high contrast feature, such as a sunspot, on the position sensor produces an analog translational error signal, and the zooming capability of the beam allows this signal to be optimized by changing the size of the high contrast feature. The error signal is used through a feedback system to rapidly adjust the tilt of the active mirror ($M9$), to eliminate image motion at all points downstream of $M9$. The technique of making spectroheliograms with a slit spectrograph is sensitive to image motion, and the improvement from use of the fast guider system is shown in Figure 5. The fast guider has a another feedback loop to the Coudé mirror ($M3$) of the coronagraph telescope, which enables the system to follow features as they rotate across the solar disk.

The final function of the MCCD optical bench is to produce calibration flat field

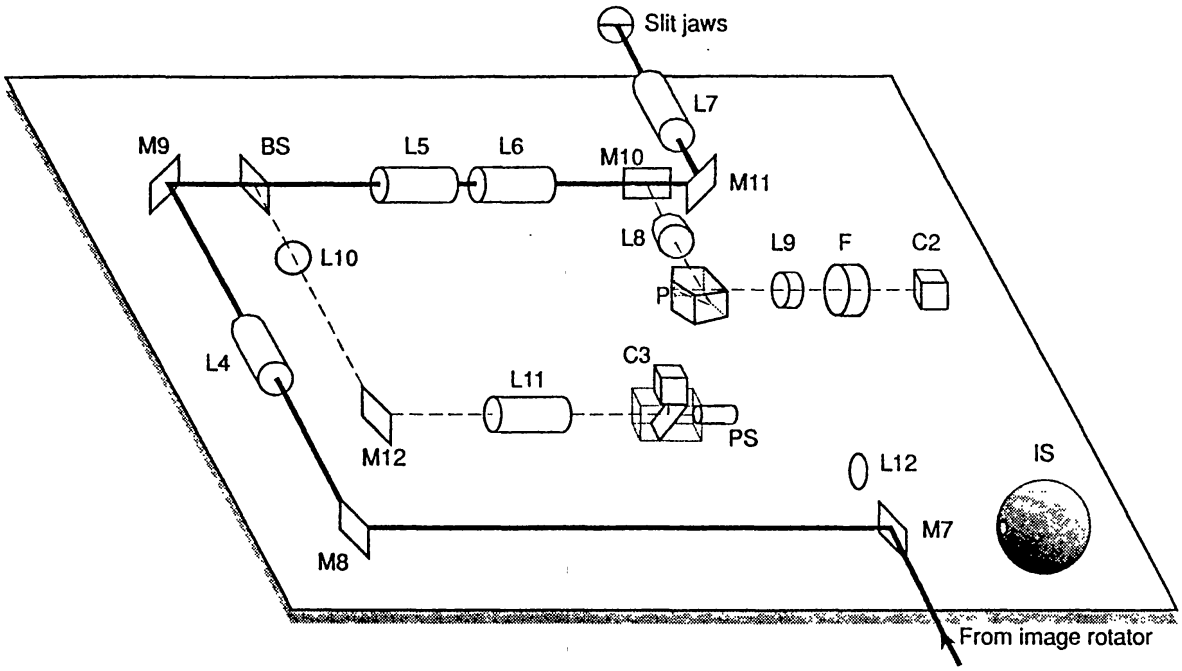


Fig. 4. The MCCD optical bench. The image rotator directs light onto the bench at $M7$. The main optical beam directs light via $M8$, through $L4$ to $M9$, through $L5$ and $L6$ to $M11$, then through $L7$ onto the spectrograph slit. The image monitor beam takes light from the closed shutter mirror $M10$, through $L8$, the pentaprism $P$, $L9$, and a narrow-band filter $F$ to the camera $C2$. The fast guider beam directs some light via the beam splitter (BS) through $L10$, off $M12$, and through $L11$ to the detector package consisting of $C3$ and the position sensor (PS). Finally, the integrating sphere (IS) and a field lens $L12$ produce a calibration image for flat fielding purposes.

images. The integrating sphere (IS) averages light from a tungsten source into all solid angles. A translation stage moves a field lens ($L12$) into the position of the first fold mirror ($M7$). The lens images the exit port of the integrating sphere at the first solar image near $M8$. This allows the calibration beam to transit the optical table in exactly the same manner as the beam from the coronagraph. The flat fielding system provides a flat spatial image, and a smoothly varying black-body spectral profile.

## 5. MCCD Modifications II – Detectors and Control Systems

At the spectrograph image plane is a Photometrics CCD camera ($C1$), a Thomson UV enhancement coated 384 × 576 pixel device. Each pixel is 22 μm on a side, which corresponds to a 0.6 arc sec pixel$^{-1}$ spatial scale. This signal is digitized to 12 bits upon readout, and the device is capable of on-chip binning. The CCD was measured to digitize 30 photoelectrons (pe) per analog-to-digital unit (ADU), with a readout noise of 41 pe. The measured dark current for the device is linear at 0.5 ADU s$^{-1}$. The CCD device is cooled to $-42$ °C with a thermo-electric system.

The image monitor bench uses a Cohu 6410 video rate CCD camera as a detector. The camera has 774 × 242 pixels, each sized 8.5 × 19.75 μm. This CCD uses frame transfer to readout the detector at video rates, and an electronic shutter allows exposure times of 0.5, 1.0, and 33 ms. This camera is not cooled.

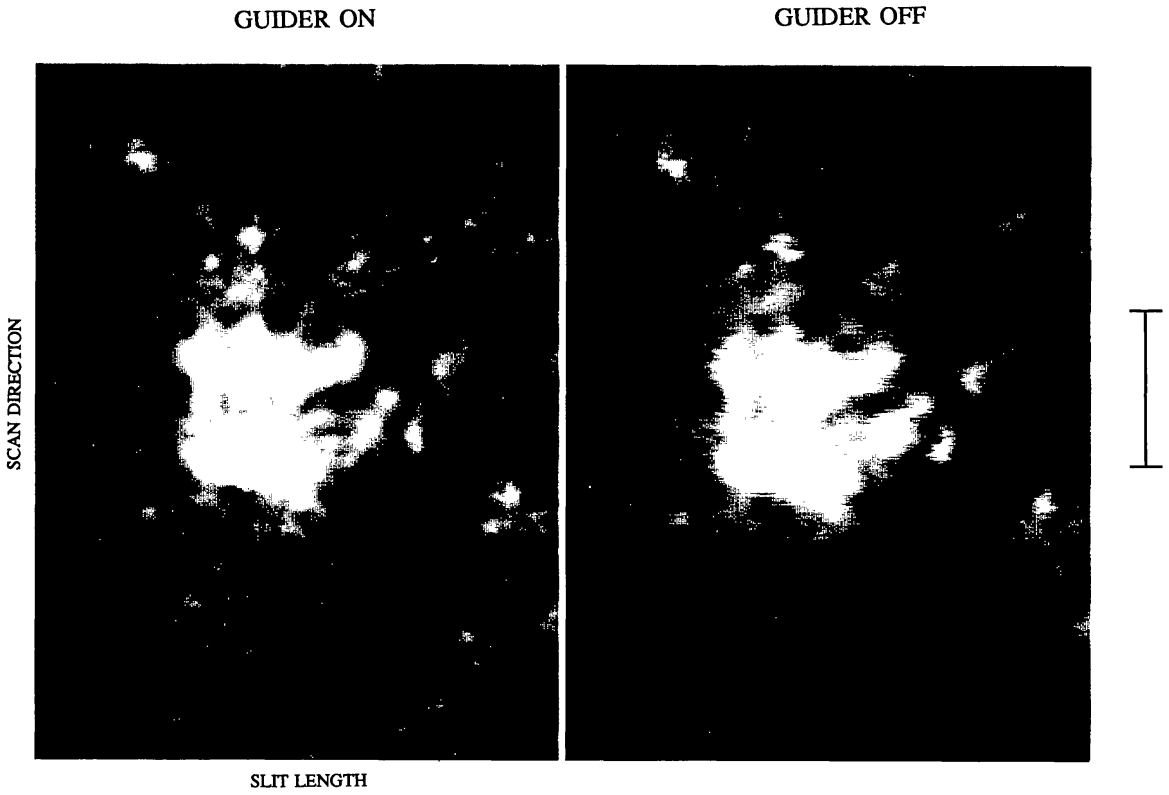


Fig. 5. The effect of the MCCD fast guider. These two sample spectroheliograms were taken with a spatial scale of 0.6 arc sec pixel$^{-1}$, a dispersion of 8 pixels Å$^{-1}$, with a slit width of 75 μm, and are centered on Hα, λ6563 Å. Each spectral frame (a single line in the image) was exposed for 75 ms, and then the image was stepped 0.6 arc sec perpendicular to the slit. Both images required about 180 s of time to compose, and were taken within 10 min of each other. The tick mark is 60 arc sec to scale. The direction along the spectrograph slit, and the direction of the scan are marked. The improvement in image quality in this case indicates that most of the image degradation arises from simple image motion, and not stretching or higher order distortions.

The control system for the MCCD is run with a 68020 based Ironics Performer 32 single board microprocessor VME system. Mounted on the VME bus are several auxiliary boards. The processor communicates with the Photometrics CC200 controller via a National Instruments GPIB VME board. Also on the VME bus is an Imaging Technology 640/2 frame grabber board, which receives the video signal from the image monitor bench Cohu camera control box, and digitizes it to a 640 × 480 pixel image, 1 byte deep. Several functions are performed by an Ironics VME Parallel Input/Output board, including driving the shutter and scanner mirrors, illuminating the tungsten filament, and moving the *M*7–*L*12 translation stage. Finally, the fast guider system is interfaced with the Ironics controller via a Datem VME BitBus board and custom electronics which control the active mirror and other elements in the fast guider beam. The system contains two 8 mm Exabyte magnetic tape drives, one accessible from the Photometrics controller, the other accessible from the Ironics.

The pSOS real-time operating system, produced by Software Components Group, Inc., is used to run the MCCD. The control system for the MCCD is written with the

*c* language in a UNIX environment, compiled into a pSOS executable kernel, and then the Ironics system is rebooted using this kernel. The pSOS control software allows direct user control of simple system tasks, such as exposing the Photometrics CCD, reading the image, and storing it to magnetic tape. Several observing modes, programmed with user defined parameters, can also be run with the software.

## 6. Observations with the MCCD Instrument

The MCCD control software offers so many user parameters that an enormous variety of observational programs are possible using the instrument. While considerably complicating the observations, this flexibility exists to allow an observing program to be defined from scientific considerations. There are 13 adjustable parameters in the MCCD system. They are number, binning, and offset of the spatial pixels, number, binning, and offset of the spectral pixels, number and size of the scan steps, exposure time, spectrograph slit width, spectrograph grating choice, spectrograph grating angle, and spectrograph prefilter. Consider the three parameters, spectral binning, slit width, and exposure. Spectral binning can be defined from a scientific consideration; namely the spectral resolution desired in the observations. Once the spectral binning is determined, it defines an optimal value for the spectrograph slit width. However, the slit width can be adjusted over a range of values and still produce satisfactory observations. When the slit width is established, it determines the amount of light entering the spectrograph and thus the exposure time required for the observations. Flexibility in the system allows trade-offs between combinations of slit width and exposure time, which can be optimized to fit best with other scientific objectives of the observing program.

The general problem of determining the observing parameters is not this simple, since no parameters form an isolated set. (In the above example, the slit width also influences the scan step size, and the exposure time affects the overall scan repetition time, and thus the optimal scan range.) The general approach is to define as many parameters as possible from the primary science objectives of the observations. The remaining parameters are balanced with one another in order to optimize the observations for the secondary science objectives. In Table I we list observational parameters for two unique observational studies. We designed the flare study to observe rapid chromospheric flares in active regions. The primary requirement for this program is the capability to observe an active region at H$\alpha$ several times each minute. Secondly, these observations must have sufficient spectral resolution and range to study the velocities found in flares, and sufficient spatial resolution to distinguish flare kernals. Unfortunately these goals work against each other, since as more pixels are used to increase the spatial and spectra resolution and range, more time is needed to read and store the data. Ultimately, trade-offs were made between the opposing goals, and the observations were configured as shown in Table I. We designed the umbral study to observe sunspot umbral oscillations with high velocity sensitivity, and thus the primary requirement of this study is very high spectral resolution. The secondary goals were to observe a small region, only a sunspot umbra, and to cadence the observations once every 60 s, to resolve the desired

TABLE I

Two sample observing studies with the MCCD

| MCCD parameter | Flare study | Umbral study |
|---|---|---|
| Spatial number | 90 | 64 |
| Spatial binning | 4 | 1 |
| Spatial offset | 0 | 0 |
| Scan number | 90 | 64 |
| Scan step size | 4 | 1 |
| Spatial range (arc sec) | 216 × 216 | 38 × 38 |
| Spatial scale (arc sec pix$^{-1}$) | 2.4 | 0.6 |
| Spectral number | 50 | 384 |
| Spectral binning | 3 | 1 |
| Spectral offset | 0 | 0 |
| Spectral range (Å) | 18.75 | 5.48 |
| Spectral dispersion (Å pix$^{-1}$) | 0.375 | 0.014 |
| Slit width (μm) | 88 | 60 |
| Grating | No. 1 | No. 2 |
| Grating angle | 11°22′ | 59°52′ |
| Spectral prefilter | ND 2.0 | No. 1004 |
| $t_{exp}$ (ms) | 25 | 600 |
| $t_{tape}$ (ms) | 55.7 | 212.3 |
| $t_{frame}$ (ms) | 130.5 | 737.8 |
| $t_{scan}$ (s) | 11.7 | 47.2 |

acoustic oscillations. Balancing these goals and other considerations, we arrived at the observing parameters listed in Table I.

The only unyielding factor in the MCCD system is the speed at which a region can be repetitively scanned. We want the time required to scan the solar image across the spectrograph slit to be as small as possible, as with all imaging spectroscopy programs using a slit spectrograph. The limits we encounter with the MCCD are of two types; limits from the continuous data storage speed, and limits from long exposure times. The time required to collect and store one frame at one slit position on the solar surface, $t_{frame}$, is given (in ms) by

$$t_{frame} = 11.79 + 0.51(N_{spat}) + 0.0038(N_{spat})(N_{spec}) + 0.0126(B_{spat} - 1) + \\ + 0.015(O_{spat}) + \mathrm{MAX}(t_{tape}, t_{exp}), \quad (1)$$

where $N_{spat}$, $B_{spat}$, and $O_{spat}$ are the number, binning and offset values of spatial pixels in the observations, $N_{spec}$ is the number of spectral pixels in the frame, and $\mathrm{MAX}(t_{tape}, t_{expos})$ is the longer of two times, either the time required to store the frame to magnetic tape, or the frame exposure time. The time required by the MCCD to write one frame to the tape system, $t_{tape}$, is given (in ms) by

$$t_{tape} = 20.57 + 0.0039(2N_{spat}N_{spec}). \quad (2)$$

In practice, the Exabyte tape storage system determines a maximum operating speed for the MCCD observations, since it is never shorter than the shortest frame exposure; the flare observations described in Table I are limited by the tape write speed. However, as shown in Equation (1), when the exposure time $t_{exp}$ exceeds the tape write time $t_{tape}$, the total frame time becomes controlled by the spectrograph exposure time. Such is the situation in the umbral observations described in Table I. Finally, the time required to complete a scan of the solar surface $t_{scan}$, is simply

$$t_{scan} = (N_{scan})\,(t_{frame})\,, \tag{3}$$

which is the product of the number of individual frames ($N_{scan}$) and the time to observe and store one frame $t_{frame}$.

We have used the new MCCD to make observations of solar active region flares in the H$\alpha$ ($\lambda$6563 Å) spectral line. Typical flare observations examine 19 Å of the solar spectrum centered on H$\alpha$, and scan a 216 × 216 arc sec region on the solar surface with a repetition rate of 12 s (see Table I). In Figure 6(a), we display sample flare spectra,

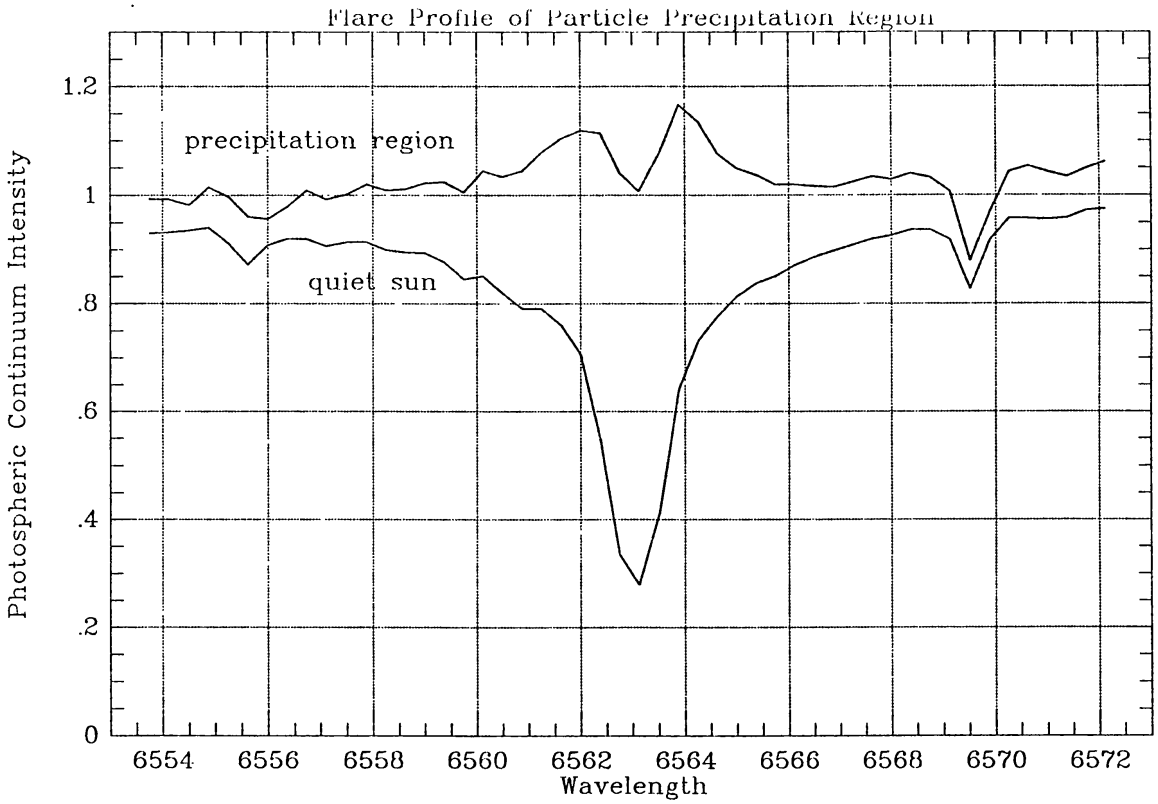


Fig. 6a. Flare observations made with the MCCD. See Table I for the observational parameters used to collect this data. In this plot we compare a quiet-Sun H$\alpha$ profile with a region showing excess emission during a flare. The emission profile suggests particle precipitation in the chromosphere (Canfield *et al.*, 1991).

which show a strong H$\alpha$ emission excess at 2.5 Å blueward of line center, characteristic of particle precipitation in the chromosphere (Canfield *et al.*, 1991). The imaging capability of the MCCD is used to determined the sites of particle precipitation, and the correspondance of these sites with flare kernels, as shown in Figure 6(b). We also make

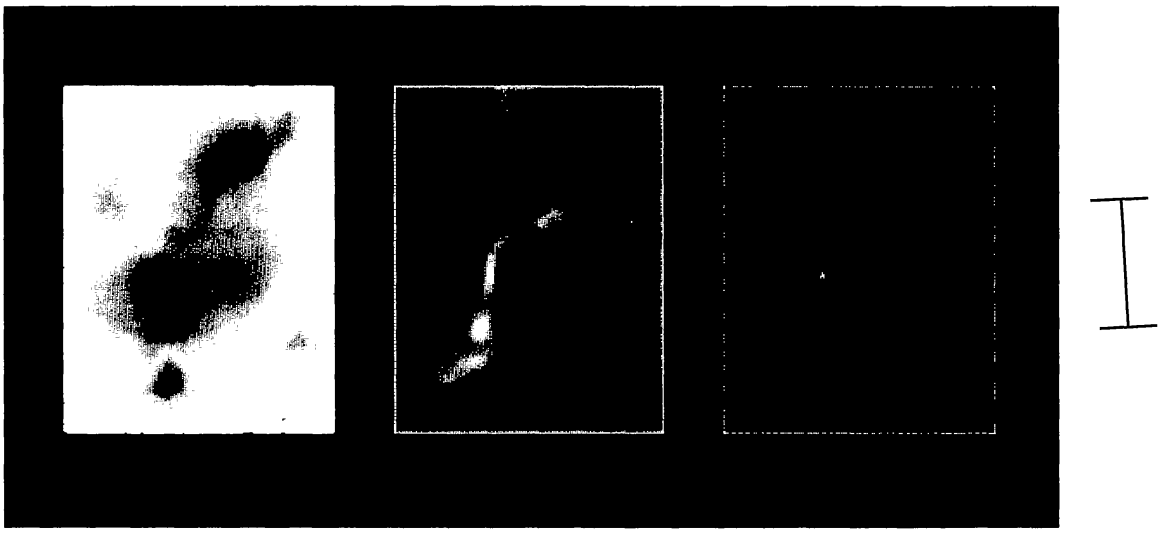

Fig. 6b. Flare spectroheliograms produced by the MCCD. The figure shows three images, produced from the same data set shown in Figure 6(a). From left to right we show a continuum image near Hα, Hα line center, and the difference from the continuum image and an image formed 2.5 Å to the blue of Hα. This last image dramatically shows the spatial location of a small region of intense particle precipitation. The tick mark is 60 arc sec to scale.

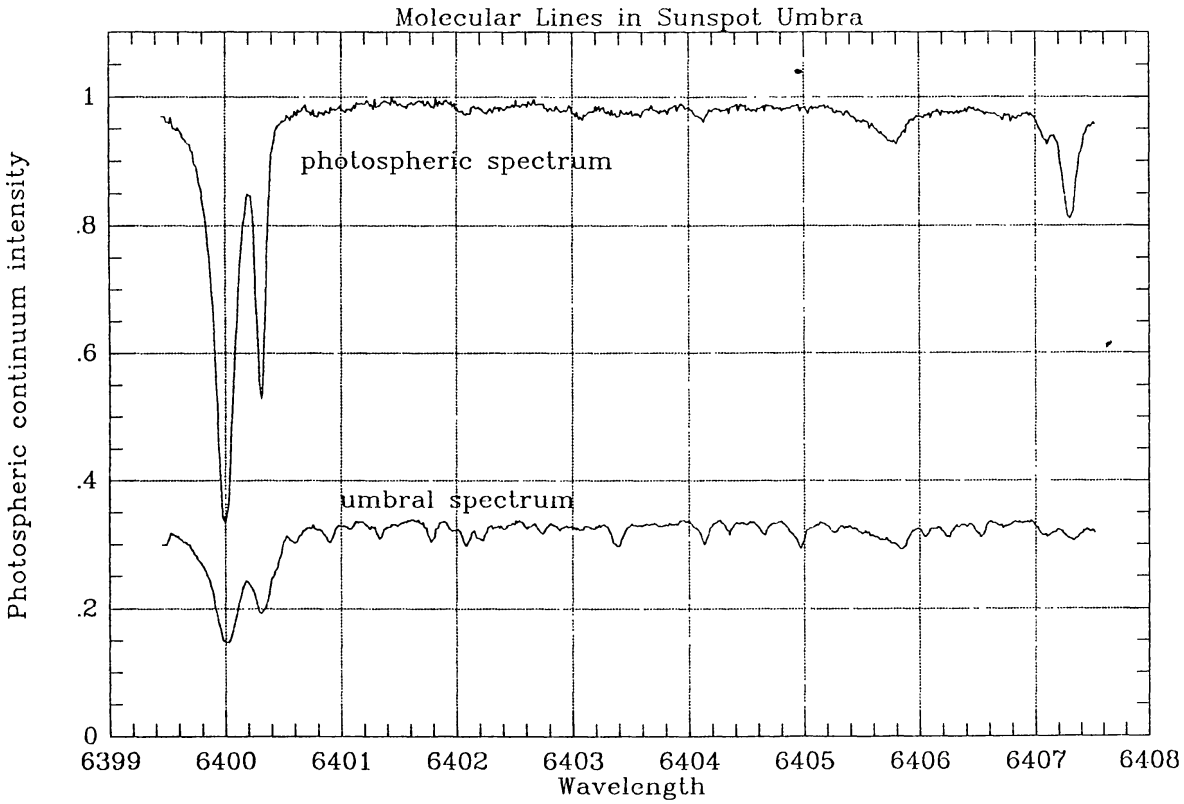


Fig. 7a. A sample spectrum of a sunspot umbra and the same spectral range of the quiet Sun, as taken with the MCCD. Visible in the umbral spectrum are several faint molecular absorption lines; the strongest four lines (λ6401.8, λ6403.4, λ6404.2, and λ6404.9) were used to measure the Doppler velocity shown in Figure 7(b).

simultaneous measurements of the vector magnetic field with the Haleakala Stokes Polarimeter (Mickey, 1985) to compare these precipitation sites with regions of current flow (Canfield *et al.*, 1991).

Another program using the MCCD system studies the oscillation modes in sunspot umbrae. We measure the velocity shifts of molecular absorption lines, which are produced only in the umbral region. Typical observations examine a 38 × 38 arc sec region centered on a sunspot umbra, and span 5 Å of the solar spectrum, centered at $\lambda$6404 Å. In Figure 7(a), we show a sample spectrum of several molecular lines seen in a sunspot umbra, which have been identified with molecules of TiO, CaH, CN, and MgO (Boyer, Sotirovski, and Harvey, 1975). The mean velocity shift of four of these lines is computed, and averaged over all umbral pixels; then the spectrograph wavelength drift is subtracted via a low-frequency temporal filter. Figure 7(b) shows a plot of the residual velocity signal and Figure 7(c) shows a power spectrum of this velocity. The high-frequency noise power in Figure 7(c), unaffected by the temporal filter, can be used to calculate the velocity error in the averaged data. The noise corresponds to a total velocity error of 3 m $s^{-1}$, and a single measurement velocity error of 95 m $s^{-1}$.

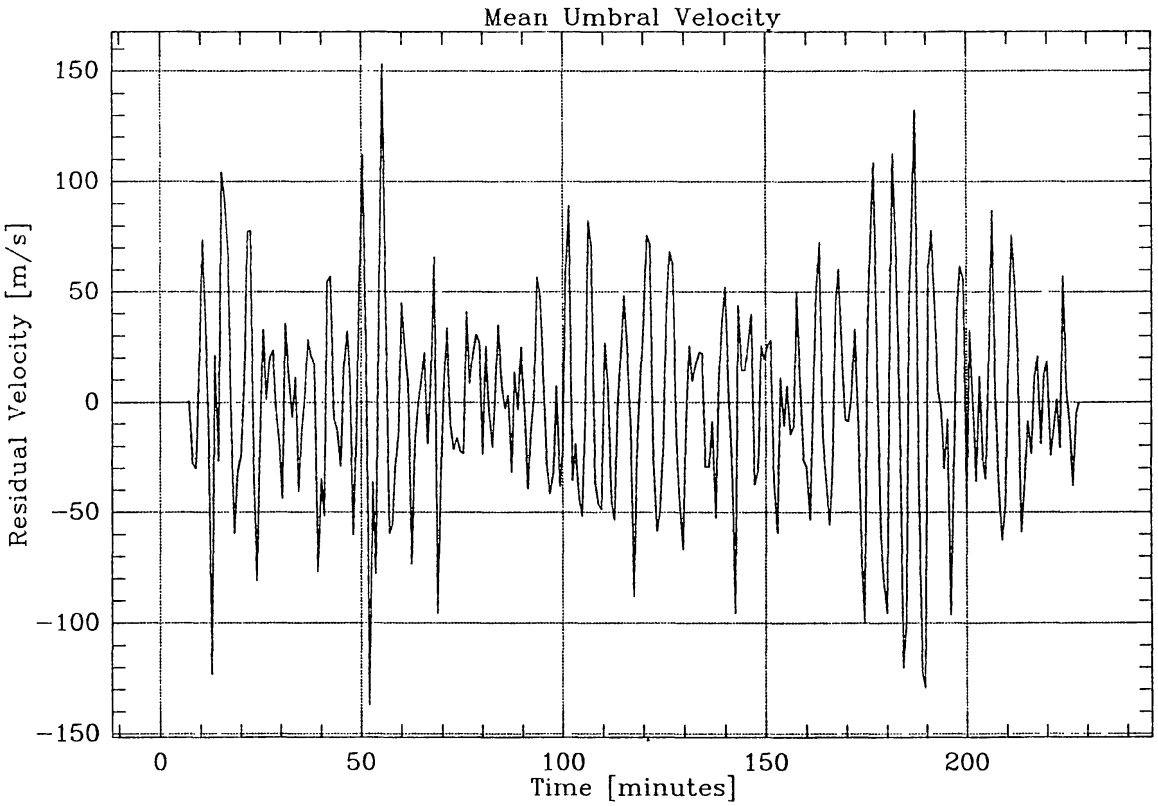


Fig. 7b. The velocity of the sunspot umbra in the main umbra of NOAA group 5836 on 15 December, 1989, as determined from Doppler shifts of the molecular lines seen in Figure 7(a). The velocity is averaged over all four lines, and over the entire umbra (260 pixels); a low-frequency temporal filter is used to subtract spectrograph wavelength drift from the original data, and we plot the residual velocity, corrected for line of sight. Just under four hours of observations are plotted.

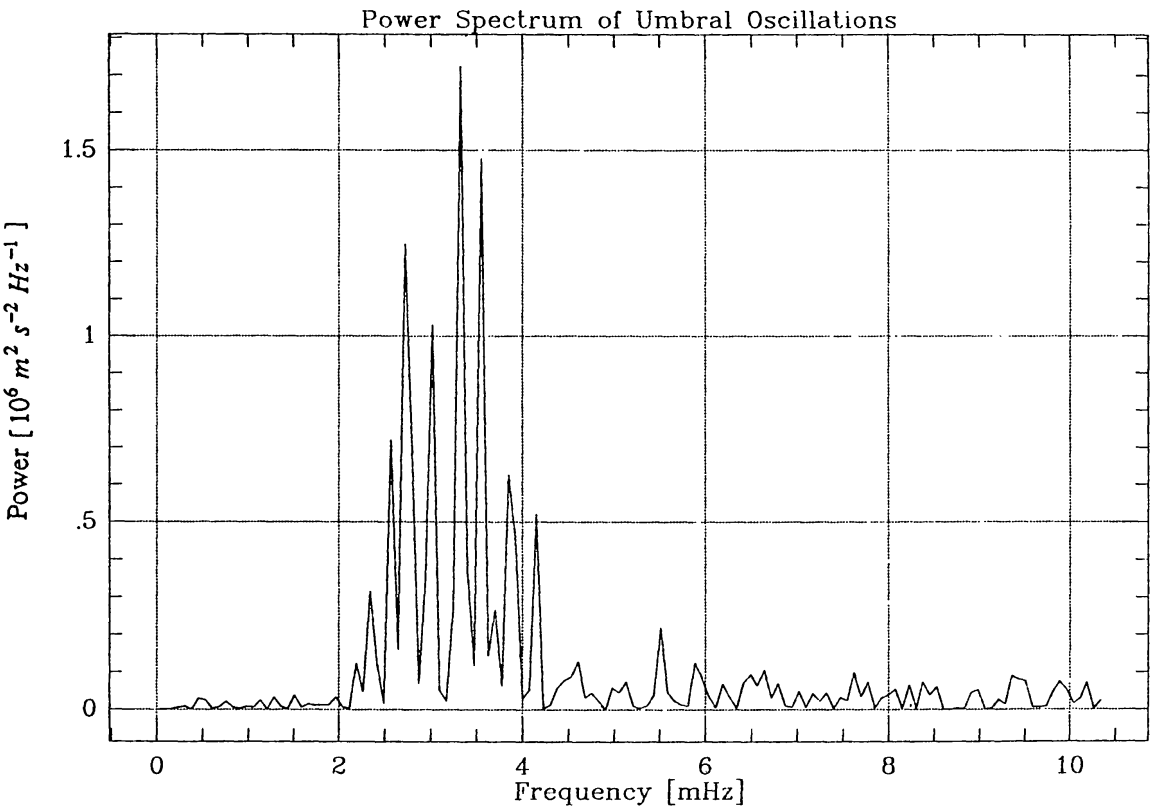


Fig. 7c. A power spectrum of the velocity signal shown in Figure 7(b). Several distinct oscillation peaks can be seen in the frequency range associated with solar *p*-mode oscillations. The high-frequency noise power in this figure implies that the noise in the velocity signal is less than 3 m $s^{-1}$.

## 7. Future Use of the MCCD

The H$\alpha$ flare study with the MCCD is planned to run through the end of this solar cycle. Each day the program is run, many hours of imaging spectroscopy data on one active region are stored. Currently, a catalog of data is being built, and only cursory glimpses at the data have been made. Along with a continuing plan to compare the data with regions of current flow from vector magnetic fields, plans exist to search for proton beam signatures with the Haleakala Stokes Polarimeter, and to compare these observations with the MCCD data.

The image monitor bench of the MCCD system is being used to observe high-degree *p*-mode intensity oscillations. We plan to correlate umbral oscillations observed spectroscopically (as in Figure 7(c)) with the absorption of *p*-modes by sunspots, as measured with the image monitor camera. Also, a program to study high-degree high-frequency *p*-mode oscillations spectroscopically is planned.

Coronal observations in Fe XIV $\lambda$5303 Å have been made. We plan to develop this program, culminating with observations during the near totality conditions that will exist on Haleakala during the 11 July, 1991 solar eclipse. We will try to develop a program to observe the corona in several lines, in order to investigate the temperature and density distribution of coronal plasma.

The MCCD system was originally designed to operate several spectrographic CCD cameras, simultaneously observing several different spectral regions. The feasibility of such a system has been demonstrated since the current system has a wide spectral range. Such multi-line observations would have the potential to study the depth dependence of energy flux in solar flares. We would be able to directly measure the propagation of acoustic energy into the solar atmosphere. We could investigate the *p*-mode absorption of sunspots in the photosphere and the chromosphere simultaneously, and make simultaneous observations of coronal plasma in several emission lines to directly determine the distribution of coronal gas at many temperatures.

## Acknowledgements

We would like to acknowledge the enormous contributions of Elaine Kiernan to the software of the MCCD, of Herb Ryerson to the design and fabrication of the fast guider electronics, and of Buzz Graves, for his design work, fabrication, installation, and general knowledge of the fast guider system. Dr Jean-Pierre Wuelser made important contributions during the characterizations of the coronagraph and spectrograph, and resolved many of the initial problems with the MCCD system. Among the list of many who have contributed to the MCCD project in important ways include Darryl Koon, Tim Georges, Les Heida and Mark Waterson at the Mees Solar Observatory, and Dr Tom Metcalf, and Chas Cavedoni at the Institute for Astronomy. Funding for this work was provided by NASA Grant NAGW 1542.

## References

Brickhouse, N. S. and Landman, D. A.: 1987, *Astrophys. J.* **313**, 463.
Boyer, R., Sotirovski, P., and Harvey, J. W.: 1975, *Astron. Astrophys. Suppl.* **19**, 359.
Canfield, R. C., Fan, Y., Leka, K. D., McClymont, A. N., Wuelser, J. P.: 1991, in L. November (ed.), *Solar Polarimetry*, National Solar Observatory, Sunspot (in press).
Fisher, R. R.: 1971a, *Solar Phys.* **19**, 431.
Fisher, R. R.: 1971b, *Solar Phys.* **19**, 440.
Fisher, R. R. and Pope, T.: 1971, *Solar Phys.* **20**, 389.
Kingslake, R.: 1983, *Optical System Design*, first ed., Academic Press, Orlando.
LaBonte, B. J.: 1986a, *Astrophys. J. Suppl.* **62**, 229.
LaBonte, B. J.: 1986b, *Astrophys. J. Suppl.* **62**, 241.
Landman, D. A.: 1976, *Solar Phys.* **50**, 383.
Landman, D. A.: 1981a, *Astrophys. J.* **244**, 345.
Landman, D. A.: 1981b, *Astrophys. J.* **251**, 768.
Landman, D. A.: 1985, *Astrophys. J.* **295**, 220.
Landman, D. A., Edberg, S. J., and Laney, C. D.: 1977, *Astrophys. J.* **218**, 888.
Landman, D. A., Illing, R. M. E., and Mongillo, M.: 1978, *Astrophys. J.* **220**, 666.
Lindsey, C. A. and Landman, D. A.: 1980, *Astrophys. J.* **237**, 999.
McCabe, M. K.: 1973, *Solar Phys.* **30**, 439.
Mickey, D. L.: 1985, *Solar Phys.* **97**, 223.